UC Irvine
UC Irvine Previously Published Works

Title

Exploiting the detector distance information in image scanning microscopy by phasor-based SPLIT-ISM.

Permalink

Journal

ISSN

Authors

Di Franco, Elisabetta

Tedeschi, Giulia

Scipioni, Lorenzo

et al.

Publication Date

DOI

Check for updates

Exploiting the detector distance information in image scanning microscopy by phasor-based SPLIT-ISM

ELISABETTA DI FRANCO,[1,2,3] GIULIA TEDESCHI,[3] LORENZO SCIPIONI,[3] ENRICO GRATTON,[3] MICHELLE DIGMAN,[3] MARCO CASTELLO,[4] ALBERTO DIASPRO,[2,5] GIUSEPPE VICIDOMINI,[6] PAOLO BIANCHINI,[2] AND LUCA LANZANÒ[1,2,7,*]

[1]*Department of Physics and Astronomy "Ettore Majorana", University of Catania, Catania, Italy*
[2]*Nanoscopy, CHT Erzelli, Istituto Italiano di Tecnologia, Genoa, Italy*
[3]*Laboratory for Fluorescence Dynamics, University of California, Irvine, USA*
[4]*R&D Department, Genoa Instruments S.r.l., Via E. Melen 83, 16152 Genova, Italy*
[5]*DIFILAB, Department of Physics, University of Genoa, Genoa, Italy*
[6]*Molecular Microscopy and Spectroscopy, CHT Erzelli, Istituto Italiano di Tecnologia, Genoa, Italy*
[7]*Centro Siciliano di Fisica Nucleare e Struttura della Materia-CSFNSM, Catania, Italy*
[*]luca.lanzano@unict.it

Abstract: Confocal microscopy is an important bio-imaging technique that increases the resolution using a spatial pinhole to block out-of-focus light. In theory, the maximum resolution and optical sectioning are obtained when the detection pinhole is fully closed, but this is prevented by the dramatic decrease in the signal reaching the detector. In image scanning microscopy (ISM) this limitation is overcome by the use of an array of point detectors rather than a single detector. This, combined with pixel reassignment, increases the resolution of $\sqrt{2}$ over widefield imaging, with relatively little modification to the existing hardware of a laser-scanning microscope. Separation of photons by lifetime tuning (SPLIT) is a super-resolution technique, based on the phasor analysis of the fluorescent signal into an additional channel of the microscope. Here, we use SPLIT to analyze the information encoded within the array detectors distance for improving the resolution of ISM (SPLIT-ISM). We find that the lateral resolution can be increased of an additional $1.3 \times$ with respect to the pixel-reassigned image with a concomitant increase in optical sectioning. We applied the SPLIT-ISM technique on biological images acquired by two currently available ISM systems: the Genoa Instruments PRISM and the Zeiss Airyscan. We evaluate the improvement provided by SPLIT-ISM through the QuICS algorithm, a quantitative tool based on image correlation spectroscopy. QuICS allows extracting three parameters related to the resolution, and contrast SNR of the image. We find that SPLIT-ISM provides an increase in spatial resolution for both the Genoa Instrument PRISM and the Zeiss Airyscan microscopes.

1. Introduction

Confocal microscopy is an optical imaging technique designed to increase the optical contrast and resolution of a sample using a spatial pinhole to block out-of-focus light in the background of the image. The pinhole is a small aperture placed in front of the detector, whose position is confocal to the illuminated spot in the specimen [1,2] and provides the optical sectioning. Its size plays a major role in determining the degree of optical sectioning and the effective resolution of the confocal microscope. The smaller the pinhole size, the better the optical sectioning and the higher the spatial resolution [3]. Unfortunately, closing the pinhole you have the disadvantage of having less light reaching the detector. Consequently, a compromise must be found to obtain an

image with good optical sectioning and spatial resolution and at the same time a good signal to noise ratio (SNR) [3].

Image Scanning Microscopy is a super-resolution technique which works in the same way as a confocal microscope but in this case the detector is replaced by an array of detectors that increases the signal to noise ratio (SNR). This array detector records, at each scan position, a small image of the illuminated region. That is why the method is named Image Scanning Microscopy [4]. Each pixel of the array acts as union of confocal pinhole and detector and records its own confocal scan image. For a detector placed at distance d from the optical axis, the one-dimensional PSF is given by:

$$PSF\left(x - \frac{d}{2}\right) \propto \exp\left[-\frac{\left(x - \frac{d}{2}\right)^2}{2\sigma_{ISM}^2}\right] \tag{1}$$

where $\sigma_{ISM} = \sigma/\sqrt{2}$, and σ is the width of the diffraction limited PSF, showing that the raw resolution of an ISM is better by a factor $\sim\sqrt{2}$ than the diffraction-limited image. Image scanning microscopy (ISM) is based on the acquisition of N_{det} images, one for each detector of the array. Once all the images have been acquired, they must be recombined into one high resolution image. The method that recombines the images is called Pixel Reassignment. All the acquired images are processed with the pixel reassignment method to obtain the final ISM image which, compared to a widefield image, has an improvement of a factor of $\sqrt{2}$ in the spatial domain. The resulting image has more signal because the images acquired by each detector in the array are added together.

Several implementations of ISM have been reported so far. All-optical implementations of ISM generate the final super-resolved image only using optical means [5–11]. In the other implementations, the final image is obtained by a computer-based reconstruction. The first experimental implementation of the Image Scanning Microscopy was made in 2010 by Müller and Enderlein, using an emCCD as detector in a confocal microscope [12]. This system recorded a scan for each position and then the data was processed by moving virtually each pixel by half its distance from the optical axis and added to a final image at the focus position of the sample and finally, this image was deconvolved to achieve a factor two improvement of the resolution given by the ISM. In 2014, a commercial version of the ISM was developed by Carl Zeiss, the Airyscan microscope [13–15]. The system is based on their standard confocal scanning microscope, but the usual point detector is replaced by a so-called Airyscan detector. This detector is based on a bundle of $N_{det} = 32$ optical fibers arranged in a hexagonal pattern. The end of each fiber is connected to one pixel of the 32 linear array multianode GaAsP-PMT. This detection scheme allows for fast readout with online signal processing [13]. In 2015, the Vicidomini group in collaboration with the Genoa Instruments company, investigated the potential of using a series of detectors (photomultipliers or avalanche photodiodes) for the Image Scanning Microscopy system, instead of using a camera for imaging as suggested by Sheppard when he proposed the method [13], to overcome the obstacle of low imaging speed. Hence, they demonstrated that good performance can be achieved with a small number of detector elements and consequently developed an ISM solution with a Single-photon avalanche diode (SPAD) array ($N_{det} = 25$), that allows to resolve the lack of integration between the spatial and temporal characteristics of the ZEISS Airyscan. Besides, the single-photon timing ability of the SPAD array made it possible to combine ISM with FLIM, thus enabling straightforward super-resolution FLIM [16].

Here, we propose a method that can further increase the resolution and optical sectioning of an ISM image by exploiting the information encoded in the distance of the detectors from the center of the array. The method is based on the Separation of photons by lifetime tuning (SPLIT) [17], a super resolution technique introduced in the context of STED microscopy based on the phasor analysis of the fluorescent signal into an additional channel of the microscope.

The first implementation of the SPLIT technique increased the spatial resolution of a STED microscope by decoding the spatial information encoded in the fluorescence lifetime [17–20]. In subsequent implementations, it has been demonstrated that the SPLIT technique can be applied using additional channels other than the lifetime [21–23]. Recently, the SPLIT technique has been applied to confocal microscopy, using the variable pinhole size of the confocal microscope as additional channel in SPLIT, that is related to the decrease in the in-focus and out-of-focus intensity [24,25]. In SPLIT-Image Scanning Microscopy (SPLIT-ISM) we use the distance of the detectors from the center of the array as the additional channel for the SPLIT technique. Along the additional channel we can distinguish two components, one corresponding to the center of the PSF and one corresponding to its periphery. SPLIT-ISM isolates the component corresponding to the center, to increase the resolution.

The generated SPLIT-ISM images were analyzed using a recent algorithm that evaluates the image quality by image correlation spectroscopy (QuICS) [26]. From this analysis, we extract the parameters R, B and N that represents, respectively, resolution (the width of the autocorrelation function), brightness (related to the image contrast) and noise (the relative noise variance, related to the SNR of the image). We show with simulations that SPLIT-ISM image can provide improved optical resolution and similar brightness with respect to the pixel-reassigned ISM image.

As an example of an application, we used SPLIT-ISM for biological imaging. Specifically, we applied it to ISM images of HeLa cells acquired using the Genoa Instruments PRISM and to ZEISS Airyscan images of MDA-MB-231, an epithelial human breast cancer cell line. We found that the SPLIT-ISM image has better resolution and contrast than the conventional PRISM and Airyscan imaging. In summary, we demonstrate that SPLIT-ISM can be used as a tool to increase the resolution of an Image Scanning Microscope.

2. Method

2.1. Cell culture and labelling

Human HeLa cells were fixed with ice-cold methanol for 20 min at –20°C and then washed three times for 15 min in PBS. After 1 h at room temperature, the cells were treated in a solution of 3% bovine serum albumin (BSA) and 0.1% Triton in PBS (blocking buffer). The cells were then incubated with rabbit anti-Tom20 polyclonal antibody (FL-145; Santa Cruz) diluted in blocking buffer at 1:100 and 1:50, respectively, for 1 h at room temperature. Cells were washed with PBS three times for 5 min each time. Secondary antibodies were applied (goat anti-rabbit IgG secondary antibody, ATTO647N (Sigma-Aldrich Merck KGaA, Darmstadt, Germania)) at a dilution of 1:500 for 1 h at room temperature. The cells were then rinsed with PBS five times for 5 min each time.

MDA MB231 cells were maintained and grown in a flask of 25 cm^2 in Dulbecco's Modified Eagle Medium (DMEM) added with 1% penicillin/streptomycin (Pen/Strep) and 10% fetal bovine serum (FBS) and maintained at 37°C and 5% CO_2. The cells were seeded on 8-well chambered coverslips and let growing until 100% confluence. Finally, we stained the cells with one drop per well of Hoechst 33342 (NucBlue Live ReadyProbes Reagent - ThermoFisher Scientific) for an hour before imaging at 37°C and 5% CO_2.

2.2. Image acquisition

ISM images were acquired using a custom ISM setup, based on what previously described in [16] and [27] and coupled with an off-the-shelf Nikon Eclipse Ti microscope body. It is equipped with several triggerable pulsed diode lasers (QuixX 488-200 PS, QuixX 642-140 PS; Omicron-laserage Laserprodukte GmbH, Rodgau, Germany). For our experiments we used the one emitting at 642 nm. The objective lens is a CFI Plan Apo VC 60× 1.49 NA oil (Nikon Instruments, Yokohama, Japan), the emission is collected by the same objective lens,

descanned, and filtered via multi-bandpass fluorescence filter (quad-line laser rejection band ZET 405-488-561-640; Chroma). The far-red fluorescence is focused on the image plane (no-pinhole) into the SPAD array, yielding at an equivalent ~1.4 AU size over the entire array. Scanning pixel size was set to about 50 nm and pixel dwell time was set to 0.2 ms, collecting $256 \times 256 \times 64$ z-stack images. In detection, we used the PRISM-Light kit for Image Scanning Microscopy (Genoa Instruments S.r.l, Genova, Italy), which includes a 25-element SPAD detector array and FPGA-based acquisition electronics. Briefly, each photon detected by each element of the SPAD array generated a digital signal that was delivered to the FPGA based data-acquisition unit through a dedicated channel. The entire custom microscope was controlled by Carma software (Genoa Instruments S.r.l, Genova, Italy), enabling the control and synchronization of all the microscope parts and devices used during image acquisition (i.e., the galvo mirrors, the laser sources and the SPAD detector array).

Airyscan Images were acquired on a Zeiss LSM 880 using an Objective Plan-Apochromat 63x/1.4 Oil DIC M27 (FWD = 0.19 mm) (Carl Zeiss Microscopy, LLC, USA). Hoechst 33342 was excited at 405 nm and its fluorescence emission detected at 460-598 nm using an array of 32 sensitive GaAsP detector elements. The pinhole of each element in the array is 0.2 A.U. The frame of the image was set at 512×512 with a zoom of 6.0 and a pixel size of 40 nm. The excitation power was kept constant unless specified otherwise. The number of line averaging was kept constant unless specified otherwise.

2.3. Simulations

Simulations of ISM images were performed in MATLAB. The object consists of filaments of tubulin in a matrix of 256×256 with a pixel size of 20 nm. We simulated a stack $I_j(x, y)$ with $j = 1 \ldots, n$, where $n = 25$, that is the number of detectors in the array and each image within the stack represents an image acquired by each detector with pinhole equal to 0.2 A.U. The Full Width Half Maximum (FWHM) size of the simulated Point Spread Function (PSF) was set to 200 nm at 1 A.U. The final images were corrupted with poissonian noise.

For comparison, we calculated the image that is obtained from the sum of all images acquired by each detector (Confocal 1 A.U.), the image acquired by the central detector (Confocal 0.2 A.U.) and the final ISM image processed with pixel reassignment (ISM image).

2.4. SPLIT-ISM algorithm

In SPLIT-ISM, we analyze the intensity at each pixel as a function of the distance of the array detectors from the center. It is known that the ISM image consists of as many images as there are detectors in the array, i.e., 25 for the SPAD array system and 32 for the ZEISS Airyscan. Each image corresponds to that acquired by a detector within the array. In the detector array (for both the SPAD array and the ZEISS Airyscan) we selected detectors that are at the same distance from the central detector, and for both systems we have 6 "rings" of detectors placed at the same distance. Therefore, instead of having a stack composed of the images acquired from each detector, we will have a stack of 6 images, where each of them is calculated as the average of all the images acquired from the detectors placed at the same distance, i.e. the detectors of the same "ring". Given this images stack $I_j(x, y)$, the images were processed with phasor analysis in which variables $g(x, y)$ and $s(x, y)$ were calculated as [28,29]:

$$g(x, y) = \frac{\sum_{j=1}^{n} I_j(x, y) \cos\left[\frac{2\pi(j-1)}{n}\right]}{\sum_{j=1}^{n} I_j(x, y)} \tag{2}$$

$$s(x, y) = \frac{\sum_{j=1}^{n} I_j(x, y) \sin\left[\frac{2\pi(j-1)}{n}\right]}{\sum_{j=1}^{n} I_j(x, y)} \tag{3}$$

where n is the number of images in the stack. The modulation and the phase are the polar coordinates of the phasor and were calculates as follows:

$$M(x, y) = [g^2(x, y) + s^2(x, y)]^{1/2} \tag{4}$$

$$\phi(x, y) = \tan^{-1} \frac{s(x, y)}{g(x, y)} \tag{5}$$

For each pixel, a fraction $f_{IN}(x, y)$ of fluorescence intensity associated with the center of the PSF was calculated by expressing the experimental phasor $P(x, y)$ as a combination of the phasors $P_{IN}(x, y)$ and $P_{OUT}(x, y)$ which represents respectively, the center and the periphery of the PSF and can be determined directly from the phasor plot. This fraction was estimated as follows:

$$f_{IN,LIN}(x, y) = \frac{[(P(x, y) - P_{IN}) \cdot (P_{OUT} - P_{IN})]}{|P_{OUT} - P_{IN}|^2} \tag{6}$$

That is proportional to the distance between the phasor P and the phasor P_{IN} along the line connecting P_{IN} and P_{OUT}. In this analysis the two phasors component P_{IN} and P_{OUT} were selected from the phasor plot. To force values of fraction to fall between 0 and 1, the values of $f_{IN,LIN}(x, y)$ are filtered through a non-linear, logistic function of the form: $f_{IN}(x, y) = 1/(1 + e^{-k_L(f_{IN,LIN}(x,y) - 1/2)})$, with $k_L = 4$, as described previously [24,25].

Finally, the SPLIT-ISM image was calculated as follows:

$$I_{SPLIT-ISM} = f_{IN}(x, y) \cdot I_{ISM}(x, y) \tag{7}$$

where $I_{ISM}(x, y)$ is the ISM image, i.e. the image obtained after pixel reassignment. Note that the image $f_{IN}(x, y)$ contains the additional spatial information (extracted from the phasor analysis of the ISM raw data) that improves the lateral resolution and optical sectioning of the SPLIT-ISM image.

2.5. Image analysis

The quality of the generated SPLIT-ISM images was analyzed the Quality by Image Correlation Spectroscopy (QuICS) algorithm [26]. The QuICS analysis was performed in MATLAB using the code available at https://github.com/llanzano/QuICS. Briefly, given an image $I(x, y)$, a two-dimensional (2D) image correlation function $G_{2D}(\delta x, \delta y)$ was calculated as:

$$G_{2D}(\delta x, \delta y) = \frac{\langle I(x, y) I(x + \delta_x, y + \delta_y) \rangle}{\langle I(x, y) \rangle^2} - 1 \tag{8}$$

where δ_x and δ_y are the spatial lag variables, $I(x, y)$ is the fluorescence intensity detected at pixel (x, y), the angle brackets indicate averaging over all the selected pixels of the image. The numerator in Eq. (8) was calculated by a 2D fast Fourier transform algorithm. The radial correlation function $G(\delta_r)$ was calculated by performing an angular mean [30]. The noise-free correlation function was estimated by performing a Gaussian fit of the correlation function $G(\delta)$ by skipping the zero-lag point:

$$G_{NF}(0) = G_{NF}(0)e^{-\frac{\delta^2}{w^2}} + G_{NF}(\infty)\delta \in [1, \delta_{max}] \tag{9}$$

Where the width parameter w corresponds to the $1/e^2$ of a Gaussian function, and it is related to the Full Width Half Maximum (FWHM) by the relationship $w = FWHM/(2 \ln 2)^{(1/2)}$; $G_{NF}(0)$

represents the amplitude; $G_{NF}(\infty)$ represents an offset value. The value δ_{max} was determined to fit a single Gaussian component. The parameters R, B, N have been calculated as:

$$R = \sqrt{2ln2}\,w \tag{10}$$

$$B = G_{NF}(0)I_{av} \tag{11}$$

$$N = \frac{G(0) - G_{NF}(0)}{G_{NF}(0)} \tag{12}$$

where we have indicated I_{av} as the average intensity value over all the pixels of the image. R is the width of the autocorrelation function, related to the spatial resolution; B is the brightness, related to the image contrast; N is the relative noise variance, related to the signal-to-noise ratio of the image [26].

The quality of an image can be analyzed by several methods [31,32]. Fourier Ring Correlation (FRC) is a popular method for measuring image resolution, which describes with a single parameter the length scale below which the image lacks significant signal content [33,34]. Compared to FRC, QuICS provides similar information via two distinct parameters: the resolution parameter R, which contains average information on the characteristic size (e.g. specimen features, effective PSF of the optical system) and the parameter N, which contains information on the noise content of the image. In this work, the use of QuICS parameters has the advantage of highlighting the effect of the SPLIT-ISM processing in terms of shrinking of the effective PSF (reduction of the parameter R) and introduction of additional noise (increase of the parameter N).

3. Results

3.1. Exploiting the ISM detector-distance information by phasor analysis

In confocal microscopy, the maximum level of resolution and optical sectioning is obtained when the pinhole is closed to 0.2 Airy Units (AU). Unfortunately, closing the pinhole, the signal to noise ratio (SNR) decreases (Fig. 1(a), top). Thus, in confocal microscopy it is necessary to find a compromise between the level of resolution and the SNR. In image scanning microscopy (ISM), this issue is resolved by substituting the pinhole with a detector array (Fig. 1(a), bottom), where each detector corresponds to a totally closed pinhole (0.2 A.U). The image is acquired for each detector to have an image with the best resolution for each acquisition, even if with low signal to noise ratio (SNR). At the end of the scan, as many images are obtained as there are detectors in the array. These images (except for the one scanned with the central detector), exhibit pixel shift due to distance from the optical axis of the microscope. Therefore, to obtain the final high-resolution image, these images must be processed with a pixel realignment algorithm, called Pixel Reassignment (PR). After running the algorithm on the images, they are added together, resulting in a high-resolution image with a high SNR (Fig. 1(a), bottom). The principle of SPLIT is shown in fig.1b. SPLIT exploits detection of intensity versus an additional channel of the microscope (e.g., lifetime, depletion power): suppose that signal originating from fluorophores located at the center of the PSF ("IN") has a different fingerprint compared to fluorophores located in the outer part of the PSF ("OUT"); in the SPLIT method the phasor analysis is used to separate the signal given by the fluorophores at the center from that given by the fluorophores at the periphery.

In SPLIT-ISM, we apply the SPLIT technique to ISM, to generate an image with a higher resolution than that obtained by the conventional PR algorithm. Specifically, we exploit the spatial information encoded in the distance of each detector from the center of the array, as shown in fig.1c (left). To apply the SPLIT method, the distance d of the detectors in the ISM array is used as an additional channel (Fig. 1(c), right). Along this channel two different components can be distinguished, one from the center of the PSF ("IN") and one from the periphery ("OUT"),
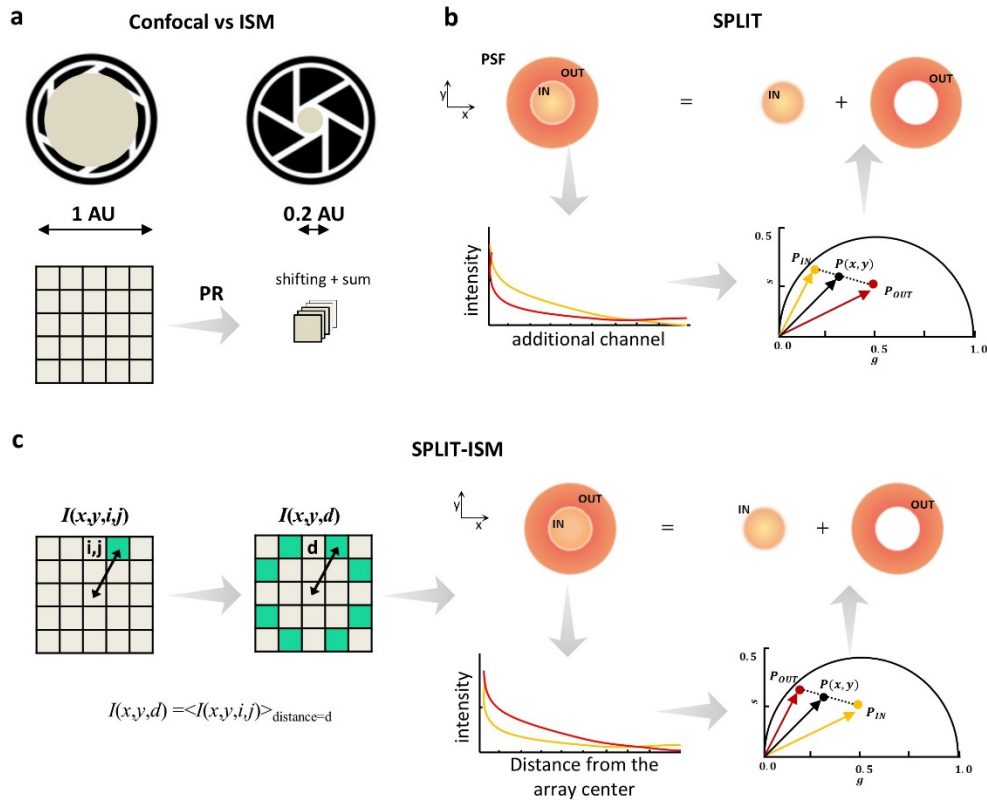
Fig. 1. Schematic principle of ISM, SPLIT and SPLIT-ISM. a) Comparison between closing the pinhole of a confocal microscope and the image formation by pixel reassignment (PR) in an image scanning microscope. b) Schematic principle of SPLIT. The fluorescence signal originating in the center of the PSF (IN) has a different fingerprint along an additional channel (e.g. lifetime) compared to the fluorescence signal originating in the periphery of the PSF (OUT). The phasor plot is used to isolate the component corresponding to the center of the PSF and generate a super-resolution image. c) Schematic principle of SPLIT- ISM: the signal from all the detectors places at the same distance from the center is averaged. Then SPLIT is applied using the detector-distance as the additional channel. The phasor plot is used to isolate the component corresponding to the center of the PSF and generate a super-resolution image.

because they have a different fingerprint. Visualization in the phasor plot [28,29] allows us to express each phasor into two components P_{IN} and P_{OUT}, that correspond to the components IN and OUT of the PSF, whose fraction $f_{IN}(x, y)$ allows us to obtain the final image SPLIT-ISM, multiplying this fraction pixel by pixel by the intensity of the final ISM image after processing it with Pixel Reassignment.
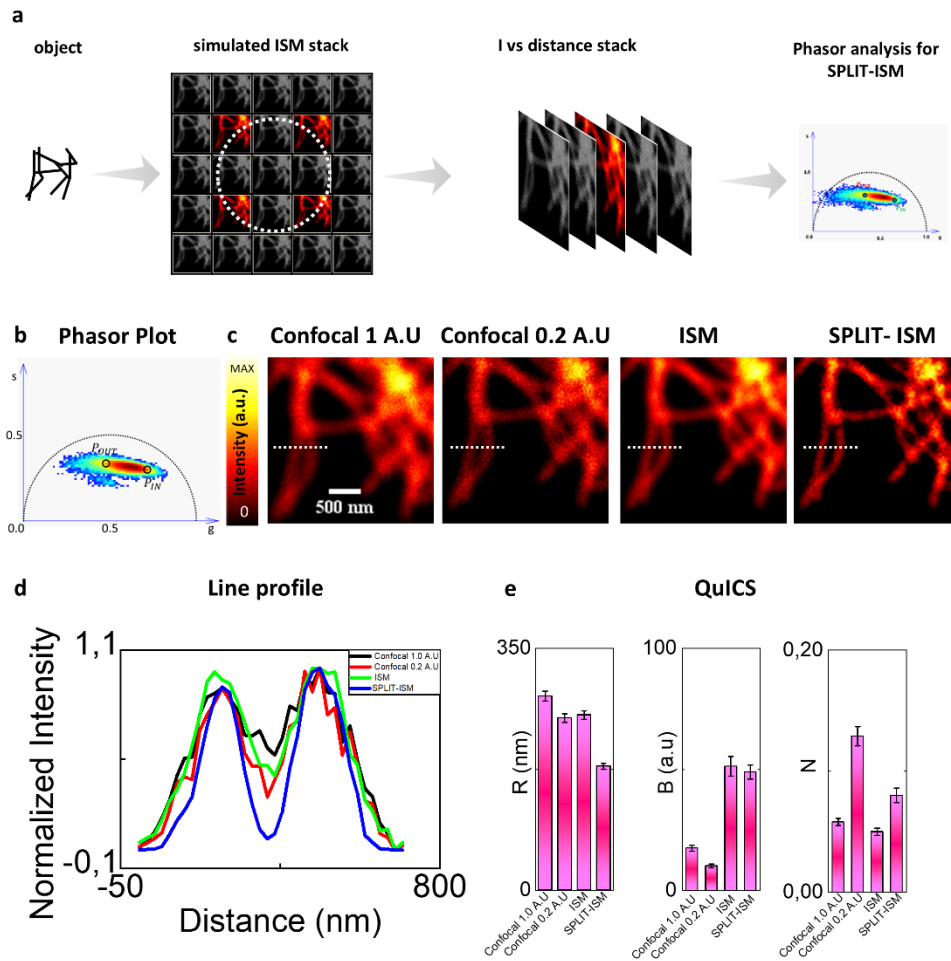
3.2. SPLIT-ISM of simulated data

Fig. 2. Validation of SPLIT-ISM by simulations. a) Schematic view of the formation of the simulated images starting from the object (resembling filaments of tubulin), then the simulated ISM stack, the stack of the intensity vs the distance, the phasor plot. b) Phasor plot in which the two phasors P_{IN} and P_{OUT} are shown. c) ROI of the simulation of the filaments of tubulin (scale bar is 500 nm): (from left to right) the confocal image at 1.0 A.U, the confocal image at 0.2 A.U, the pixel reassignment image and the SPLIT-ISM image. d) Line profile corresponding to the dashed line in c). e) Evaluation of resolution (R), Brightness (B) and the noise level (N) by the QuICS algorithm.

Through simulated data (Fig. 2(a) shows the creation of the simulation), we evaluated the improvement given by the SPLIT-ISM method compared with an ISM image. We simulated an ISM image of tubulin filaments, as shown in Fig. 2(c), and we made a comparison between the

image resulting from the sum of all images acquired by each detector of the array (corresponding to a Confocal image with 1 A.U. pinhole size), the image of the central detector (corresponding to a Confocal image with 0.2 A.U. pinhole size), the pixel reassignment image (hereafter called ISM image) and the image obtained through application of the SPLIT-ISM (hereafter called SPLIT-ISM image).

The phasor components P_{IN} and P_{OUT} have been selected directly from the phasor plot (Fig. 2(b)). First, to verify if the SPLIT-ISM technique led to an improvement of the ISM image, we performed a line profile analysis (Fig. 2(c)) and we found the full width half maximum (FWHM) values, through a Gaussian fit, which were used to estimate the resolution. The results are shown in Table 1 (σ is the standard deviation).

Table 1. Line profile analysis on simulated ISM images.

Number of samples	Tubulin filaments Simulation	Resolution (nm)	$\sigma_{Resolution}$
10	Confocal 1.0 A.U.	199	21
10	Confocal 0.2 A.U.	169	23
10	ISM	170	26
10	SPLIT-ISM	123	25

As expected, the resolution of the ISM image is comparable to that of the confocal at 0.2 A.U. but higher than that of the confocal at 1 A.U. The resolution of the SPLIT-ISM image is ~1.3× (~40 nm) higher than the resolution of the ISM image. To obtain a more statistically robust result, the QuICS algorithm was applied on 10 different simulations. The QuICS algorithm provides the 3 parameters of Resolution (R), Brightness (B), and Noise (N) (Fig. 2(e)). Through QuICS we found that the resolution for the SPLIT-ISM image is $R = (180 \pm 4)$ *nm*, the brightness is $B = (49 \pm 3)$ *a.u.* and the noise is $N = 0.080 \pm 0.006$ compared to the ISM image whose QuICS parameters are: $R = (254 \pm 6)$ *nm* - $B = (51 \pm 4)$ *a.u* - $N = 0.050 \pm 0.003$. For the 1 A.U. image and for the 0.2 A.U. image we have, respectively, that $R = (280 \pm 7)$ *nm* - $B = (17.5 \pm 1)$ *a.u.* - $N = 0.058 \pm 0.003$ and $R = (250 \pm 6)$ *nm* - $B = (10 \pm 0.8)$ *a.u.* - $N = 0.129 \pm 0.008$. This analysis confirms that the SPLIT-ISM image has better resolution than the ISM image. Note that the value of R provided by QuICS represents the average size of the features in the image and is larger than the FWHM obtained by the line profile analysis. Regarding the brightness, we note that both ISM and SPLIT-ISM have better brightness than the other two images. Finally, the SPLIT-ISM image has a noise level which is higher than that of the ISM image. Indeed, the SPLIT-ISM image contains the additional noise introduced by the fraction image $f_{IN}(x, y)$ (see Eq. (7)).

We also estimated the resolution using decorrelation analysis [32], a more widely used method compared to QuICS. As shown in Supplement 1 Table 1, this analysis confirms that the SPLIT-ISM image has better resolution than the ISM image.

3.3.　SPLIT-ISM of data acquired with the Genoa Instruments PRISM

Next, we verified if the technique could be applied to a biological system. Images of mitochondria in HeLa cells were acquired using a SPAD array ISM setup. The microscope is based on a PRISM Genoa Instruments system, which implements a 5×5 squared SPAD-array detector, that generated 25 images. To obtain the fraction f_{IN}, we choose the phasors P_{IN} and P_{OUT} directly from the phasor plot and we set the two phasors as: $P_{IN} = (0.29; 0.36)$ and $P_{OUT} = (0.17; 0.24)$ (Fig. 3(a)). In principle, the P_{IN} and P_{OUT} components could be determined, more rigorously, by imaging diffraction-limited objects (e.g. small beads) and measuring the phasors corresponding to the central and outer part of the PSF. On the other hand, direct selection in the phasor plot has the convenience of skipping this calibration step.

Next, we obtained the SPLIT-ISM image that is compared to the image obtained summing all images from the array (confocal 1.0 A.U.), the central detector of the ISM (confocal 0.2 A.U.) and
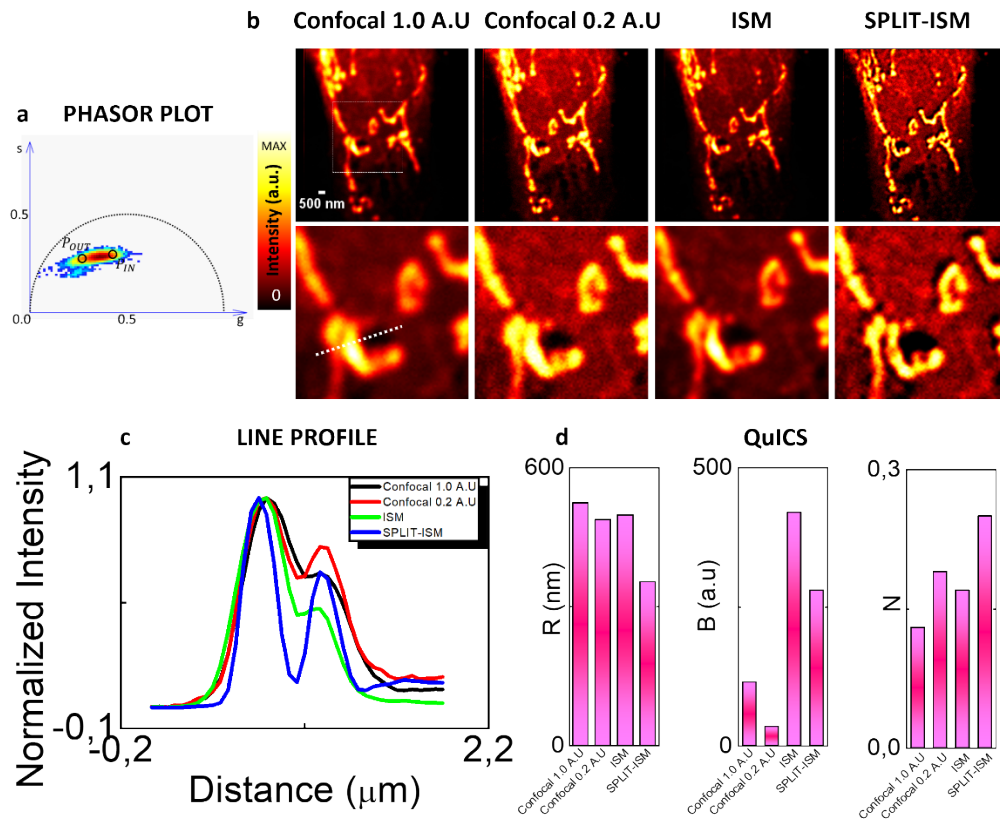
Fig. 3. Application of the SPLIT-ISM to PRISM images of mitochondria in fixed HeLa cells. a) Phasor plot in which the two phasors P_{IN} and P_{OUT} are shown (xy plane). b) The images show on the xy plane and ROIs of the same images: (from left to right) the confocal image at 1.0 A.U, the confocal image at 0.2 A.U, the pixel reassignment image and the SPLIT-ISM image. c) Line profile corresponding to the dashed line in b). d) Evaluation of resolution (R), Brightness (B) and the noise level (N) by the QuICS algorithm.

the pixel reassignment image (ISM image) (Fig. 3(b)). To make the comparison we performed a line profile, and we calculated the three parameters with QuICS algorithm. From the line profile (Fig. 3(c)) it can be seen that SPLIT-ISM provides the best spatial resolution. QuICS confirmed that SPLIT-ISM improves the resolution (see Table 2). As shown in Supplement 1 Table 2, also decorrelation analysis confirmed that the SPLIT-ISM image has better resolution than the ISM image.

Table 2. QUICS analysis of the images acquired with the Genoa Instruments PRISM.

XY Image	Resolution (nm)	Brightness (a.u)	Noise
Confocal 1.0 A.U.	524	15	0.13
Confocal 0.2 A.U.	488	35	0.19
ISM	398	420	0.17
SPLIT-ISM	354	280	0.25

We also analyzed the *xz* section of the image, using the same phasors P_{IN} and P_{OUT}, as shown in Supplement 1 Fig. S1. We made a line profile along z to observe the effect of the SPLIT-ISM processing on this direction. As can be seen in Supplement 1 Fig. S1, the SPLIT-ISM technique provides improved optical sectioning. Quantitatively, we performed the QuICS algorithm, to obtain the parameters of resolution (R), brightness (B), and noise (N). We calculated the resolution also using a gaussian fit on the line profiles, for *xy* (ISM: R = 333 *nm*; SPLIT-ISM: R = 232 *nm*) and *xz* (ISM: R = 550 *nm*; SPLIT-ISM: R = 315 *nm*) sections of the image, as shown in Supplement 1 Fig. S2.

3.4. SPLIT-ISM of data acquired with the ZEISS Airyscan

Finally, the SPLIT algorithm was also applied to the images acquired using the ZEISS Airyscan detector, which is based on the same operating principle of ISM but with a different shape of the detector array. Instead of having the square SPAD array, in this case we have a hexagonal shaped array with 32 GaAsP PMTs detector elements. We apply the SPLIT algorithm to Airyscan images of MDA-MB-231 cell nuclei labelled with Hoechst 33342. Also in this case, we generate the fraction f_{IN} by choosing the phasors P_{IN} and P_{OUT} directly from the phasor plot. As seen in Fig. 4(a), the chosen values of P_{IN} and P_{OUT} are respectively $(0.11; 0.17)$ and $(0.01; 0.09)$. The image obtained by performing the pixel reassignment with the ZEISS ZEN software which supplies the super-resolved image is thus multiplied by the image obtained from the f_{IN} fraction and the SPLIT-ISM image is obtained. Figure 4(b) compares the 1.25 A.U confocal image (which corresponds to the image obtained by adding the 32 images acquired by the ZEISS detector), the 0.2 A.U confocal image (which corresponds to the image of the central detector element), the super-resolved Airyscan image and the SPLIT-ISM image.

A line profile analysis shows, qualitatively, that SPLIT-ISM method improves the resolution of the image (Fig. 4(c)).

To have a more quantitative and statistical result, also in this case we applied the QuICS algorithm. From the obtained results (Fig. 4(d)), we see that the proposed method leads to an improvement in resolution (Airyscan: R = 440 ± 10 *nm*; SPLIT-ISM: R = 333 ± 7 *nm*) and a slight increase in the noise level (Airyscan: N = 0.13 ± 0.001; SPLIT-ISM: N = 0.14 ± 0.005). We note that, in this case, we observe a large increase in brightness from the Airyscan to the SPLIT-ISM image. This is probably related to the presence of out-of-focus signal in the Airyscan image, which is removed in the SPLIT-ISM image.

In addition, we performed multiple line profiles on different points of the images and performed Gaussian fits to find the value of the FWHM, as shown in Supplement 1 Fig. S3. We estimated that the resolution improvement is around 60 nm (ISM: R = 411 ± 17 nm; SPLIT-ISM: R = 347 ± 17 nm).
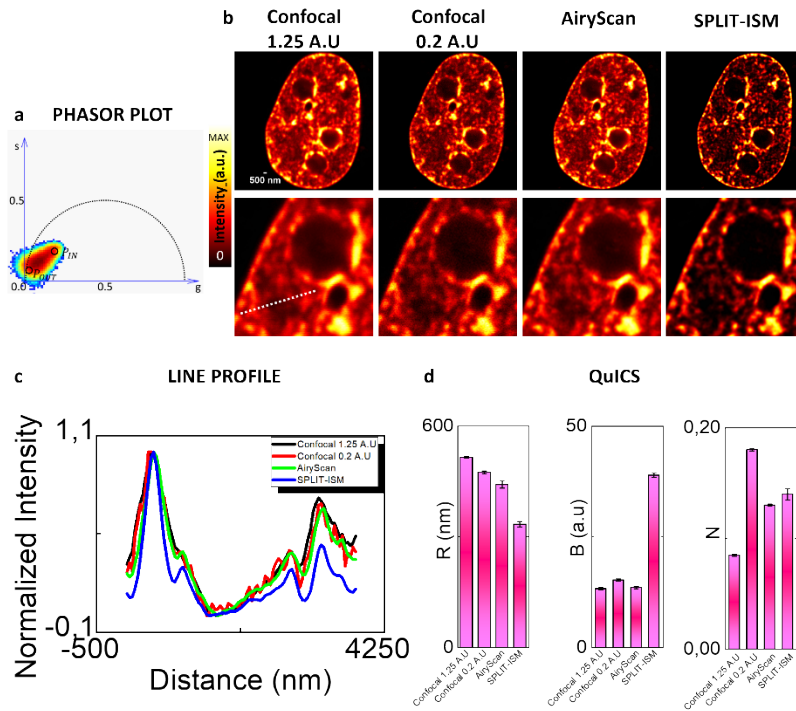
Fig. 4. Application of SPLIT-ISM to Airyscan images of live MDA-MB231 cell nuclei. a) Phasor plot in which the two phasors P_{IN} and P_{OUT} are shown. b) The images show (from left to right) the confocal image at 1.25 A.U, the confocal image at 0.2 A.U, the pixel reassignment image and the SPLIT-ISM (SPLIT-ISM) image and the ROI (dashed square) of the images. c) Line profile corresponding to the dashed line in b). d) Evaluation of resolution (R), Brightness (B) and the noise level (N) by the QuICS algorithm.

4. Discussion

Confocal microscopy is an imaging technique that improves resolution and removes out-of-focus signal compared to widefield microscopy. It has been demonstrated that the optical sectioning of a confocal microscope can be improved by phasor analysis and the Separation of Photon by lifetime tuning (SPLIT) technique, using a tunable pinhole, overcoming the limitation of confocal microscopy, in which there is a drastic decrease in the signal-to-noise ratio in the case of pinhole at 0.2 A.U, using the technique called SPLIT-PIN [24,25]. This limitation can also be overcome in Image Scanning Microscopy, in setups in which the point detector has been replaced by a detector array that behaves like a pinhole system at 0.2 A.U [13,16]. In these setups, the SNR reduction given by the closed pinhole is overcome by the number of detectors present in the array, obtaining an image with better optical sectioning and better lateral resolution by a factor $\sqrt{2}$ without sacrificing SNR.

Here, we demonstrated that we could achieve a further improvement in spatial resolution in ISM using phasor analysis and SPLIT algorithm [17] exploiting the detector distance information. To the best of our knowledge, this is the first time that phasor analysis is used to improve spatial resolution in imaging scanning microscopy. Even though SPLIT-ISM is conceptually similar to SPLIT-PIN, in SPLIT-ISM the data from the different detectors are acquired simultaneously whereas the tuning of pinhole size in SPLIT-PIN requires a sequential acquisition. However, we note that there are other ways to process the intensity detected from the array to improve the performances of ISM. For instance, it has been shown recently that improved resolution and

contrast in ISM can be achieved using a high-performance deconvolution method, the SPITFIR(e) method, by dividing the detector array into 3 sub-detectors [35].

Using simulations of an ISM image, we observed that SPLIT-ISM can produce an image with better resolution than both the confocal image and the (pixel-reassigned) ISM image. We estimated a resolution improvement of ∼ 40 nm with respect to the ISM image. Having obtained this result, we applied it to the images coming from the Genoa Instruments PRISM and Zeiss Airyscan systems and confirmed experimentally the improvement of resolution provided by SPLIT-ISM. This also suggests that the SPLIT-ISM technique can be applied to ISM systems of different geometry. In the future, it would be interesting to apply the algorithm to systems with a higher number of detectors (e.g. the square 7×7 PRISM by Genoa Instruments) to see if this could lead to an additional improvement in the phasor analysis. Finally, we demonstrated that SPLIT-ISM can be applied to images of biological samples acquired with an image scanning microscopy setup, using the spatial information deriving from the distance of the detectors present in the array from the central one, outlining the "rings" of detectors that are at the same distance. We believe that SPLIT-ISM can be used in the future for different applications in the study of chromatin to understand its behavior and to study it under different treatments.

References
1. A. Diaspro, P. Bianchini, F. Cella Zanacchi, *et al.*, "Fluorescence Microscopy," in (2019), pp. 1039–1088.
2. J. B. Pawley, "Fundamental Limits in Confocal Microscopy," in *Handbook Of Biological Confocal Microscopy* (Springer US, 2006), pp. 20–42.
3. C. J. R. Sheppard, X. Gan, M. Gu, *et al.*, "Signal-to-Noise Ratio in Confocal Microscopes," in *Handbook Of Biological Confocal Microscopy* (Springer US, 2006), pp. 442–452.
4. I. Gregor and J. Enderlein, "Image scanning microscopy," Curr. Opin. Chem. Biol. **51**, 74–83 (2019).
5. A. G. York, P. Chandris, D. D. Nogare, *et al.*, "Instant super-resolution imaging in live cells and embryos via analog image processing," Nat. Methods **10**(11), 1122–1126 (2013).
6. A. G. York, S. H. Parekh, D. D. Nogare, *et al.*, "Resolution doubling in live, multicellular organisms via multifocal structured illumination microscopy," Nat. Methods **9**(7), 749–754 (2012).

7. A. Curd, A. Cleasby, K. Makowska, *et al.*, "Construction of an instant structured illumination microscope," Methods **88**, 37–47 (2015).

8. S. Roth, C. J. Sheppard, K. Wicker, *et al.*, "Optical photon reassignment microscopy (OPRA)," Opt. Nano. **2**(1), 5 (2013).

9. G. M. R. De Luca, R. M. P. Breedijk, R. A. J. Brandt, *et al.*, "Re-scan confocal microscopy: scanning twice for better resolution," Biomed. Opt. Express **4**(11), 2644 (2013).

10. G. De Luca, R. Breedijk, R. Hoebe, *et al.*, "Re-scan confocal microscopy (RCM) improves the resolution of confocal microscopy and increases the sensitivity," Methods Appl. Fluoresc. **5**(1), 015002 (2017).

11. T. Azuma and T. Kei, "Super-resolution spinning-disk confocal microscopy using optical photon reassignment," Opt. Express **23**(11), 15003 (2015).

12. C. B. Müller and J. Enderlein, "Image Scanning Microscopy," Phys. Rev. Lett. **104**(19), 198101 (2010).

13. J. Huff, W. Bathe, R. Netz, *et al.*, *The Airyscan Detector from ZEISS Confocal Imaging with Improved Signal-to-Noise Ratio and Superresolution* (2015).

14. L. Scipioni, L. Lanzanó, A. Diaspro, *et al.*, "Comprehensive correlation analysis for super-resolution dynamic fingerprinting of cellular compartments using the Zeiss Airyscan detector," Nat. Commun. **9**(1), 5120 (2018).

15. K. Korobchevskaya, B. Lagerholm, H. Colin-York, *et al.*, "Exploring the Potential of Airyscan Microscopy for Live Cell Imaging," Photonics **4**(3), 41 (2017).

16. M. Castello, G. Tortarolo, M. Buttafava, *et al.*, "A robust and versatile platform for image scanning microscopy enabling super-resolution FLIM," Nat. Methods **16**(2), 175–178 (2019).

17. L. Lanzanò, I. Coto Hernández, M. Castello, *et al.*, "Encoding and decoding spatio-temporal information for super-resolution microscopy," Nat. Commun. **6**(1), 6701 (2015).

18. G. Tortarolo, Y. Sun, K. W. Teng, *et al.*, "Photon-separation to enhance the spatial resolution of pulsed STED microscopy," Nanoscale **11**(4), 1754–1761 (2019).

19. L. Lanzanò, L. Scipioni, M. D. Bona, *et al.*, "Measurement of nanoscale three-dimensional diffusion in the interior of living cells by STED-FCS," Nat. Commun. **8**(1), 65 (2017).

20. I. Coto Hernández, M. Castello, G. Tortarolo, *et al.*, "Efficient two-photon excitation stimulated emission depletion nanoscope exploiting spatiotemporal information," Neurophotonics **6**(04), 1 (2019).

21. I. Cainero, E. Cerutti, M. Faretta, *et al.*, "Chromatin investigation in the nucleus using a phasor approach to structured illumination microscopy," Biophys. J. **120**(12), 2566–2576 (2021).

22. S. Pelicci, G. Tortarolo, G. Vicidomini, *et al.*, "Improving SPLIT-STED super-resolution imaging with tunable depletion and excitation power," J. Phys. D: Appl. Phys. **53**(23), 234003 (2020).

23. M. J. Sarmento, M. Oneto, S. Pelicci, *et al.*, "Exploiting the tunability of stimulated emission depletion microscopy for super-resolution imaging of nuclear structures," Nat. Commun. **9**(1), 3415 (2018).

24. M. D'Amico, E. Di Franco, E. Cerutti, *et al.*, "A phasor-based approach to improve optical sectioning in any confocal microscope with a tunable pinhole," Microsc. Res. Tech. **85**(9), 3207–3216 (2022).

25. E. Di Franco, A. Costantino, E. Cerutti, *et al.*, "SPLIT-PIN software enabling confocal and super-resolution imaging with a virtually closed pinhole," Sci. Rep. **13**(1), 2741 (2023).

26. E. Cerutti, M. D'Amico, I. Cainero, *et al.*, "Evaluation of sted super-resolution image quality by image correlation spectroscopy (QuICS)," Sci. Rep. **11**(1), 20782 (2021).

27. I. Nepita, S. Piazza, M. Ruglioni, *et al.*, "Image Scanning Microscopy to Investigate Polycomb Protein Colocalization onto Chromatin," Appl. Sci. **13**(3), 1556 (2023).

28. L. Malacrida, S. Ranjit, D. M. Jameson, *et al.*, "The Phasor Plot: A Universal Circle to Advance Fluorescence Lifetime Analysis and Interpretation," Annu. Rev. Biophys. **50**(1), 575–593 (2021).

29. M. A. Digman, V. R. Caiolfa, M. Zamai, *et al.*, "The Phasor Approach to Fluorescence Lifetime Imaging Analysis," Biophys. J. **94**(2), L14–L16 (2008).

30. L. Scipioni, A. Rossetta, G. Tedeschi, *et al.*, "Phasor S-FLIM: a new paradigm for fast and robust spectral fluorescence lifetime imaging," Nat. Methods **18**(5), 542–550 (2021).

31. R. Dosselmann and X. D. Yang, "A comprehensive assessment of the structural similarity index," Signal Image Video Process **5**(1), 81–91 (2011).

32. A. Descloux, K. S. Grußmayer, and A. Radenovic, "Parameter-free image resolution estimation based on decorrelation analysis," Nat. Methods **16**(9), 918–924 (2019).

33. G. Tortarolo, M. Castello, A. Diaspro, *et al.*, "Evaluating image resolution in stimulated emission depletion microscopy," Optica **5**(1), 32 (2018).

34. N. Banterle, K. H. Bui, E. A. Lemke, *et al.*, "Fourier ring correlation as a resolution criterion for super-resolution microscopy," J. Struct. Biol. **183**(3), 363–367 (2013).

35. S. Prigent, S. Dutertre, A. Bidaud-Meynard, *et al.*, "A comparison of high resolution image reconstruction methods from confocal array detector with a new deconvolution algorithm," bioRxiv (2022).